Bringing multidisciplinary geosciences into quantitative inversion: A Midland Basin case study

Olivier Winter[1], Ahmed Mohamed[1], Anna Leslie[1], Gabino Castillo[1], Hassan Odhwani[1], Trevor Coulman[1], Francisco Brito[1], Adriana Perez[1], Vishnu Pandey[1], Cesar Marin[1], and Chi Vinh Ly[1]

Abstract

Over the last two decades, the driver behind the boom in unconventional reservoirs has been the development of horizontal drilling and hydraulic fracturing. More recently, the fall in oil prices has resulted in the industry refocusing on the shale market and its most profitable plays, a notable example being the Permian Basin. We argue that this refocusing should also take place in the technology domain and that seismic and its derivatives should provide reservoir and completion engineers with the means to optimize well planning. This is illustrated with a case study of an advanced quantitative interpretation workflow tailored for a seismic multiclient program in the Wolfberry Play of the Midland Basin. Seismic imaging begins by providing a structural interpretation basis, then quantitative interpretation provides 3D elastic and geomechanical attributes through prestack inversion and azimuthal inversion, respectively. This 3D canvas of elastic attributes is combined with petrophysical, mineralogical, geomechanical, and geochemical properties measured at the wells. The challenge of reconciling such data sets with different scales and spatial sampling is overcome using physical, empirical, or statistical relationships within the data. The adjunction of rock data to the 3D elastic attributes provides calibration and validation of the inversion results. More interestingly, it allows for quantitative prediction of lithology, facies, porosity, and geochemical properties away from the wells. The purpose of the resulting calibrated reservoir model is to assist in optimizing drilling plans and executing completion designs.

Introduction

The Midland Basin is located on the eastern edge of the Permian Basin (Figure 1). Although the structure of the subsurface is relatively flat, the geology is far from simple as the surveys overlay the Eastern Shelf of the basin in the east and the Horseshoe Atoll in the north. The formations of interest, the Spraberry and Wolfcamp, are commonly referred to as the Wolfberry Play. Figure 1c displays a simple stratigraphy of the area. The depth of the zone of interest ranges from 6000 to 8000 ft, which corresponds roughly to 1.1 to 1.5 s in two-way seismic time. In this paper, we discuss the specific implementation of a multidisciplinary geoscience workflow for quantitative interpretation of the Spraberry and Wolfcamp unconventional plays. The Hobo/Gypsy multiclient programs discussed here were acquired in 2016 and 2017 in two phases and span 500 mi^2 in Howard and Martin counties, Texas.

To image these formations, seismic data acquisition is widely used, providing 3D coverage of the subsurface. Traditionally, seismic data have been used in horizon interpretation for identifying structure and computing various seismic attributes related to phase, frequency, and amplitude. These attributes are used for mapping the extent of reservoirs away from wells with a greater degree of certainty.

With the availability of full-offset data and survey aspect ratios approaching unity, combined with a carefully designed processing sequence, seismic data are not only being used for amplitude variation with offset (AVO) analysis for detection of hydrocarbons, but also for amplitude variation with azimuth (AVAz) analysis that relates to fractures and geomechanical properties. AVO/AVAz simultaneous inversion is based on the Knott and Zoeppritz formulation, which states that variation of the reflectivity with the angle of incidence is a function of elastic properties of the layers above and below the interface. Simultaneous inversion produces elastic properties over the seismic volume at seismic resolution.

In addition, the Permian Basin's rich history (oil was first struck in the Midland Basin in 1921) provides a wealth of drilling-related geologic information. Using wells that have wireline logs available, it is common to build a petrophysical model of each formation using the rock sample data as calibration and validation points. In this study, by collecting rock samples from the wells with wireline data available, mineralogy and geochemistry data for each formation can be related to the wireline in the petrophysical model and provide richer information on mineralogy and organic content (Peake et al., 2014). This multidisciplinary framework, combined with 3D elastic volumes from the seismic inversions, can help in predicting rock properties away from the well logs.

The first section of this paper describes the building of the petrophysical model, the novelty of our application lying in the inclusion of mineralogical and geochemical data during this process. The second section describes the seismic methods, explaining the salient features of acquisition and processing that will lead to stable and trustworthy isotropic and anisotropic inversion products. We explain how prior information and petrophysics can be used to improve initial models and for validation during this phase. The last section will describe and further discuss the integration of the two previous phases in the presence of mineralogy and geochemical information. Different interpretation and data analytics techniques provided 3D volumes of engineering-oriented attributes such as geologic facies, porosity, brittleness, and organic content maturity and quality. These attributes assist in the optimal planning of well location, orientation, and completion for maximum return on investment.

Geology and rock physics

Rock samples. During the early stage of the work, core samples and cuttings were gathered along with borehole wirelines. Traditionally, X-ray diffraction analysis (XRD) of core plugs would

[1]CGG.

https://doi.org/10.1190/tle37030173.1.

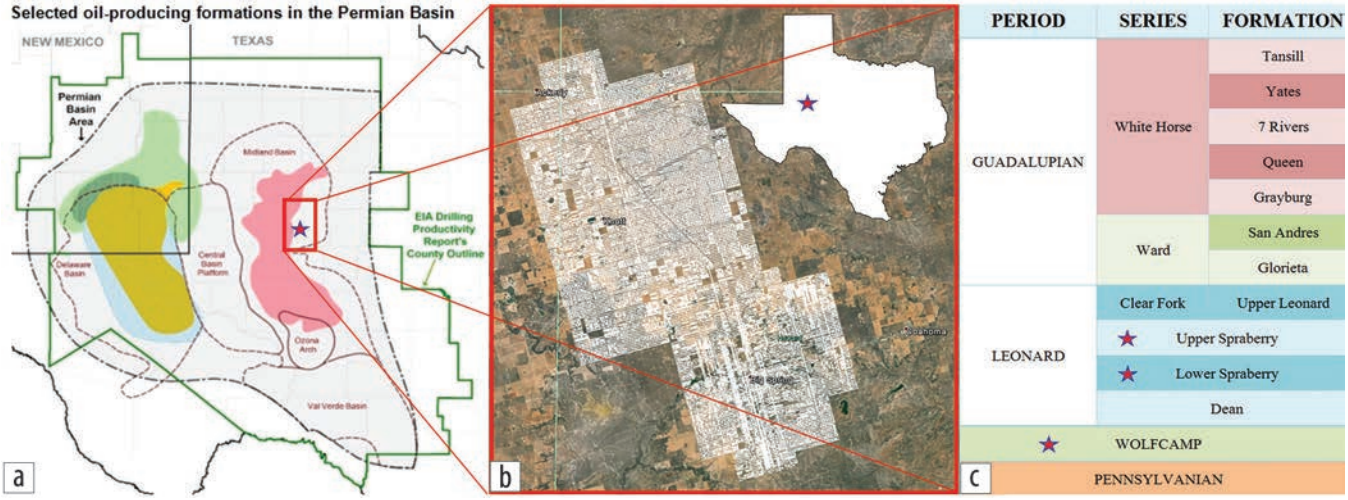

Figure 1. (a) Map of the Permian Basin and its subdivision in the Delaware and Midland basins, from U.S. Energy Information Administration. (b) Position map of the seismic acquisition layout. (c) Simplified stratigraphy of the Midland Basin.

be collected; later we describe how cuttings can yield further mineralogical and geochemical information.

Mineralogy. As cuttings samples are usually collected as part of the drilling process, and there are fewer cores being drilled in the United States, it is easier to collect geographically distributed cuttings material rather than cores to increase understanding of geologic heterogeneity in the survey area. The analysis of approximately 500 ditch-cuttings samples was carried out using a RoqScan instrument, which is an automated mineralogical analysis tool. The instrument is based on a mobile scanning electron microscope (SEM) with a built-in energy dispersive spectrometry (EDS) detector to provide elemental analysis. SEM-EDS applied to mineralogical analysis uses a motor-driven stage in an SEM equipped with one to four EDSs. The SEM-EDS used at the well site is a rugged version of this technology, using specialized hardware and software to generate elemental compositions at specific points on samples. Pixel-by-pixel image analysis and EDS chemical signatures from the SEM platform provide spatially resolved mineral speciation. This provides data at finer resolutions than bulk analysis techniques (XRD and X-ray fluorescence), which irradiate a large surface area of the sample, yielding a cumulative response (Ashton et al., 2013).

Samples were prepared by solvent removal of volatile hydrocarbons and low-temperature drying. The cleaned and dried samples (cuttings or core) were mounted in an acrylic sample holder, ground flat with 1200 grit in water or alcohol, then sputter coated with a layer of carbon under vacuum. The viscosity of the acrylic in which the cuttings were immersed was sufficient to prevent settling and ensured that the analyzed surfaces were randomly oriented. Electron beams generated in the SEM's vacuum chamber imaged the sample and generated the elemental composition data. Topography-sensitive secondary electrons, generated as the electron beam strikes the sample surface, were collected by the detector for computer imaging. X-rays generated during scanning are characteristic of the elements from which they were generated, providing a qualitative atomic composition of the sample. A dictionary listing of mineral phases with associated elemental suites was then utilized to associate the concentration amount of the analyzed specimens to a mineralogy type, and this was provided for each sample in the analysis and plotted against the well logs for calibration.

The mineralogical data generated from the cuttings were then used to derive a brittleness index as per the Jarvie et al. (2007) formulation. The results from this calculation showed the Wolfcamp C Formation to consistently be the most ductile due to higher clay content in the lower portion of the formation. This significant change in the mineralogy and calculated ductility is a clear marker for the shift from the Wolfcamp C carbonate rock into a clastic rock type. The brittleness of the other Wolfcamp and Spraberry zones are closely correlated to the carbonate component in these formations. The mineralogical data were then used to help constrain the log-derived petrophysical mineral model, such that the final log-derived mineral model is ground truthed.

Additionally, a high-resolution photomicrograph was generated from each sample analyzed, which allowed for examination of the rock fabric and texture as well as the pore size, shape, and structure to be qualified. The rock texture data were then used to constrain and understand the wireline log data and possible rock effects on the quality of the logs for editing purposes.

Geochemistry. Geochemical attributes are the second kind of data we recovered from rock samples for this survey. Geochemical evaluation and petroleum system modeling (1D) were part of the integrated workflow for seismic reservoir characterization as shown in Figure 2. The information available from different wells was combined with the data derived from geochemical analyses performed on cuttings and core samples collected from wells across the study area. These analyses included total organic carbon (TOC) determination, pyrolysis, and organic petrography (reflectance measurements). This provided insight into the source rock quality across the study area and, through 1D petroleum systems modeling, allowed the thermal evolution of the Wolfcamp and Spraberry formations to be evaluated within the study area. This new integration was performed for the following purposes: (1) to evaluate the geochemical properties of the Wolfcamp and Spraberry formations and integrate these into the petrophysical model (TOC values); (2) to improve the understanding of hydrocarbon generation at

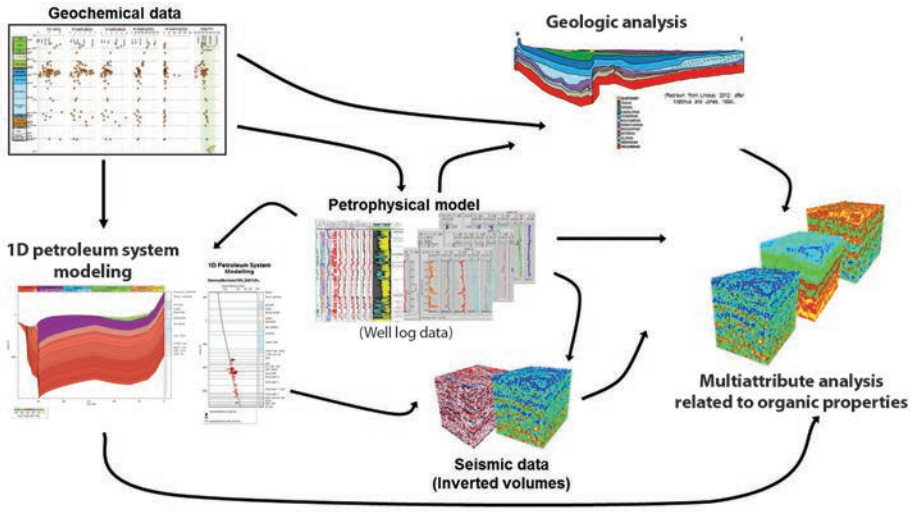

Figure 2. Simplified workflow used in the Permian Basin for multiattribute analysis.

different well locations across the study area; (3) to predict geochemical properties away from the wells by the integration of geochemical data and seismic attributes from inverted volumes; and (4) to contribute to the understanding of the hydrocarbon potential of the Wolfcamp and Spraberry formations.

Organic rock properties like TOC were integrated into the petrophysical model by conversion of the TOC to the equivalent in kerogen volume. This data helped to establish the mineral volume for further analysis. 1D basin modeling led to improved understanding of hydrocarbon generation at different well locations across the study area. From this analysis we obtained calibrated maturity curves from eight well locations.

Overall, the organic properties of the Wolfcamp and Spraberry formations in most of the wells evaluated were shown to be of good quality for generating hydrocarbons based on TOC, S2, and hydrocarbon index (HI) values. Different intervals from the Wolfcamp Formation (A, B, C, and D) showed a TOC average ranging from 1.74 to 6.47 wt% (weight percentage average by intervals), and the highest values were most often obtained in Wolfcamp A and D. The Spraberry Formation showed TOC value averages ranging from 1.28 to 4.11 wt%, and the highest values were most consistently obtained in the Upper Spraberry Formation. A change in the HI values index was observed between the Spraberry and Wolfcamp formations. Overall, the highest values (better quality–oil prone) were displayed in the Spraberry Formation, though both the Wolfcamp and Spraberry formations showed a maturity level within the oil window, confirming the intervals as shale oil plays in the survey. In most of the wells evaluated, the Wolfcamp Formation indicated early to peak maturity stage, and early maturity stage for the Spraberry Formation. The maturation process decreased the original organic properties of the evaluated formations. Therefore, the measured values represent the remaining properties of the organic matter.

Petrophysics. Petrophysics includes not only conventional estimation of complex mineralogy, porosity, and water saturation, but also integration with core and cuttings data, pore pressure analysis, and rock physics reconstruction of compressional and shear (P and S) sonic logs for evaluation of geomechanical properties, elastic properties, and seismic well ties. Out of 16 wells used to tie the seismic, five contained the high-quality data required for calibration points within the study area. These included dipole sonic logs, conventional core analysis, including XRD, and on seven of the wells, cuttings were gathered and analyzed specifically for this study. Edited logs were used in all phases of the study, and synthetic logs were generated to enhance sparse data sets, particularly in those wells lacking S-sonic data.

Cuttings provide mineralogical control for wells lacking core data and were also used to verify existing XRD data in key wells. In addition, the cuttings provided textural information through analysis of pore geometry, and they were linked to geomechanical properties through generation of a brittleness index and to the geochemical properties via organic proxies from trace elements. In data-poor wells, cuttings sampled every 30 ft provided average mineralogy trends, which were matched with the petrophysical evaluations of lithology.

Using a combination of matrix inversion and maximum likelihood estimation (Mitchell and Nelson, 1988), mineralogy was estimated from the simultaneous solution of well log response equations with uncertainties assigned to each input. Differences between input well logs (gamma ray, density, neutron, photoelectric factor, and resistivity) and curves reconstructed from mineralogical outputs were minimized. As suggested by available control, volumes for major constituents (clay, quartz, calcite, pyrite, and kerogen) were generated, while minor components were ignored. For the kerogen volume, the estimation is compared to estimates of TOC from core analysis and from Schmoker (1979) to ensure it was reliable. The lithologic model also estimated total and effective porosity and used modified Simandoux (1963) to obtain water saturation (Poupon and Leveaux, 1971). Rock physics, in the form of the self-consistent model (Berryman, 1980), was then applied to these volumes to match P- and S-sonic data in control wells, followed by application of the calibrated model to wells lacking sonic curves. P- or S-sonic logs were not used in lithology estimation, thus avoiding circular logic in reconstructing these curves. Rock physics increases the number of wells available for well ties, seismic inversion, and geomechanical modeling, and also provides a final check of prior editing. Figure 3 shows a crossplot of V_P/V_S as a function of P-impedance for seven lithotypes identified in the Wolfcamp and Spraberry formations. The cutoff applied for a given lithotype is unique to each geologic interval.

Pore pressure prediction represents an integral part of stress analysis in conjunction with isotropic and azimuthal inversion and is also utilized in geomechanical modeling. Integration of bulk density gives vertical stress (σV), while pore pressure provides the means of finding effective stress. Elevated pore pressure (in excess of hydrostatic pressure) is found from trend analysis of the

P-sonic log, using a variant of Eaton's (1976) method. Assuming horizontal transverse isotropy (HTI), horizontal stresses and normal compliance were calculated as a function of Poisson's ratio and Young's modulus, using isotropic and azimuthal inversion outputs (Gray et al., 2012).

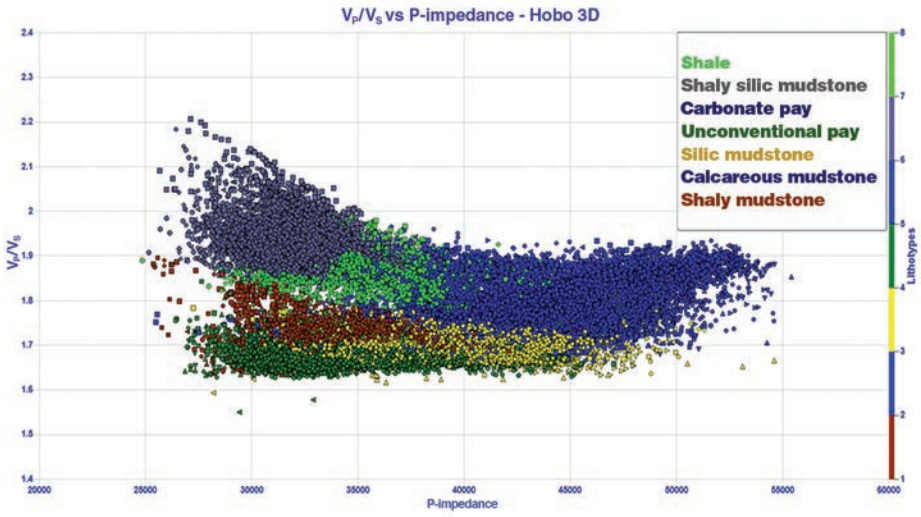

Figure 3. V_P/V_S ratio versus P-impedance crossplots for lithotypes within the Wolfcamp and Spraberry formations. Cutoffs are formation dependent.

Seismic: Acquisition, processing, and quantitative interpretation

After having collected rock physics data, the second piece of the puzzle is the seismic technique itself. Here we describe (1) the aspects of acquisition and processing that have the greatest impact on reservoir interpretation; (2) the reservoir preconditioning, a crucial part of the transition between imaging and interpretation; and (3) the isotropic and azimuthal inversions.

Acquisition and amplitude-preserved imaging. Early on, in the design phase, special care was given to acquire sufficient inline and crossline offsets so that all azimuths would feature angles of incidence of 40° or more. We obtained the most reliable estimation of incidence angles for a given offset through ray tracing using P-sonic logs in the area of interest. Receiver and shot spacings were selected according to the Fresnel zone at the shallowest targets and based on studies of previous data to identify the maximum frequency expected at these levels. Full acquisition parameters and methods are described by Coulman et al. (2017). Low-frequency signal is important for quantitative interpretation (Yates et al., 2016), so special care was taken by using a broadband, nonlinear vibrator sweep starting at 3 Hz and by accounting for geophone and instrument responses prior to deconvolution.

The seismic imaging sequence was optimized to deliver data ready for reservoir interpretation. Statics were derived using a tomographic model of the near surface computed from first arrival times. The surface wave noise, "ground roll," was adaptively removed using local spatial transforms with true geographic coordinates that take into account the nonuniformity of seismic sampling on land. A surface consistency constraint was applied on scaling, deconvolution, and residual statics computation. Prior to migration, the volume was 5D interpolated onto a denser grid to provide uniform offset-vector tiles (OVT) for the migration. The main goal of the interpolation was to provide a regular OVT basis for the migration algorithm. Using OVT domain migration ensured that the data were migrated in an offset- and azimuth-compliant manner. To reconstitute accurate amplitudes for all azimuths, the migration used a time-domain orthorhombic algorithm, accounting for VTI and HTI anisotropic effects (Wang and Wilkinson, 2012). After migration, each OVT contained a single-fold volume that had a unique source-to-receiver vector offset. This was the ideal domain in which to begin reservoir preconditioning.

Preconditioning for quantitative interpretation. The Spraberry and Wolfcamp horizons are sandwiched between two harder layers, the Clearfork on top and the Canyon/Strawn below. The top layer acts as a strong multiple generator. In addition, there is relatively little impedance contrast within the reservoir layers, leading to low reflectivity. Coupled with this, the seismic multiples generated from the bounding lithologies within the reservoir layer are particularly severe and make imaging the reservoir itself quite problematic, as seen in Figure 4. A 3D multiple attenuation module was used to split the gathers into six azimuths and run multiple attenuation on the individual azimuths in the tau-p domain. When looking at the common-depth-point (CDP) gathers, moveout of 80 ms in the negative direction (up) and 80 ms in the positive direction (down) is considered to be interfering multiples.

Amplitude tomography compensates for the amplitude (energy) loss caused by seismic attenuation. A tomographic inversion approach using depth-domain image gathers can be utilized to compensate for amplitude loss in reflection data due to attenuation. At this stage, the common-offset-vector domain data were projected to the angle/azimuth domain. Next, curvelet-domain noise attenuation was employed to attenuate noise in the angle-azimuth domain. Small residual moveout may still be present in the data after prestack time migration (PSTM), which can be corrected by the application of time-variant trim statics. Trim statics compute the crosscorrelation between an individual trace within a CDP and its pilot (usually a stack of the traces in the CDP). This helps improve gather flatness beyond that which anisotropic PSTM can produce. Here, time-variant trim statics were computed on azimuth angle gathers, as prestack inversion requires flat gathers after normal moveout, otherwise slope and intercept attributes are contaminated. Wavelet transform-based resolution enhancement incorporates structural conformity constraints and sparse regularization into an inversion-based deconvolution. This method provides a resolution-enhanced, broader bandwidth image with improved signal-to-noise ratio and geologic coherence. A prestack conformal method was used in this case to preserve the AVAz response. The module maintains the measured AVAz response throughout the process.

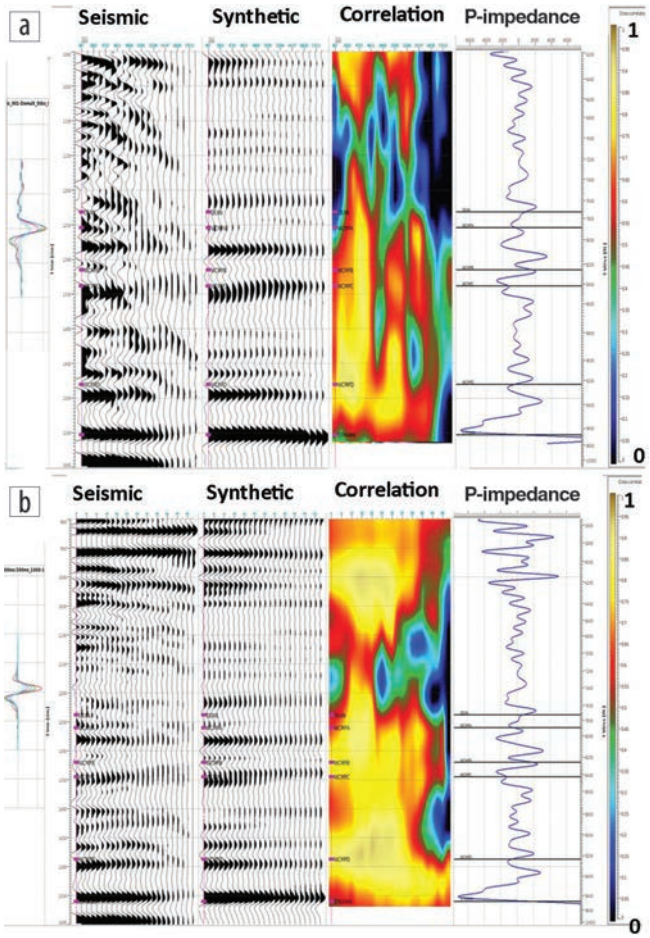

Figure 4. Prestack well tie (a) before conditioning and (b) after conditioning. From left to right, seismic angle gather, synthetic angle gather, correlation coefficient, and P-impedance. The overall correlation coefficient increased from 67% to 78% after conditioning.

At each of the aforementioned steps in the preconditioning, AVO compliancy was checked by computing crosscorrelations between synthetic gathers computed from sonic logs and the actual seismic gathers at the well head location, to ensure this process was not detrimental to the correlation coefficient. Figure 4 shows an example of a prestack well tie with a synthetic versus actual seismic comparison before and after preconditioning. Other AVO-specific prestack controls were implemented, using gradient and intercept attributes as described by Lacombe et al. (2017).

Isotropic inversion. Prestack seismic inversion for elastic properties leads to increased resolution through removal of tuning effects. Another benefit is the conversion of interface properties such as reflectivity to layer-based properties: P-impedance, S-impedance, and V_P/V_S, which are absolute values and therefore easier to interpret. The inversion used a constrained sparse spike inversion (CSSI) algorithm (Russell and Hampson, 1991). The CSSI inversion is absolute and therefore requires a low-frequency model (LFM) to fill the low-frequency gaps, which are not present in the seismic data. This is why the recovery of low-frequency signal through acquisition and processing was emphasized before: to reduce reliance on the LFM and let the seismic fill more of the gap (Yates et al., 2016). In this case, low frequencies in the data were present to 3 Hz. The inversion is usually done within a limited time range, allowing the assumption of a stationary wavelet. In this case, the inversion window was defined from the Clearfork Formation to the Canyon Formation (Pennsylvanian in Figure 1) to encompass the zone of interest.

During the inversion, the forward modeling requires wavelets. For this work, one wavelet was extracted for each of the five angle stacks. The LFM generation and wavelet extractions were supported by well-to-seismic ties, as shown previously in Figure 4. Figure 5 shows the section view of absolute P-impedance, S-impedance, and V_P/V_S ratio volumes overlaid with well

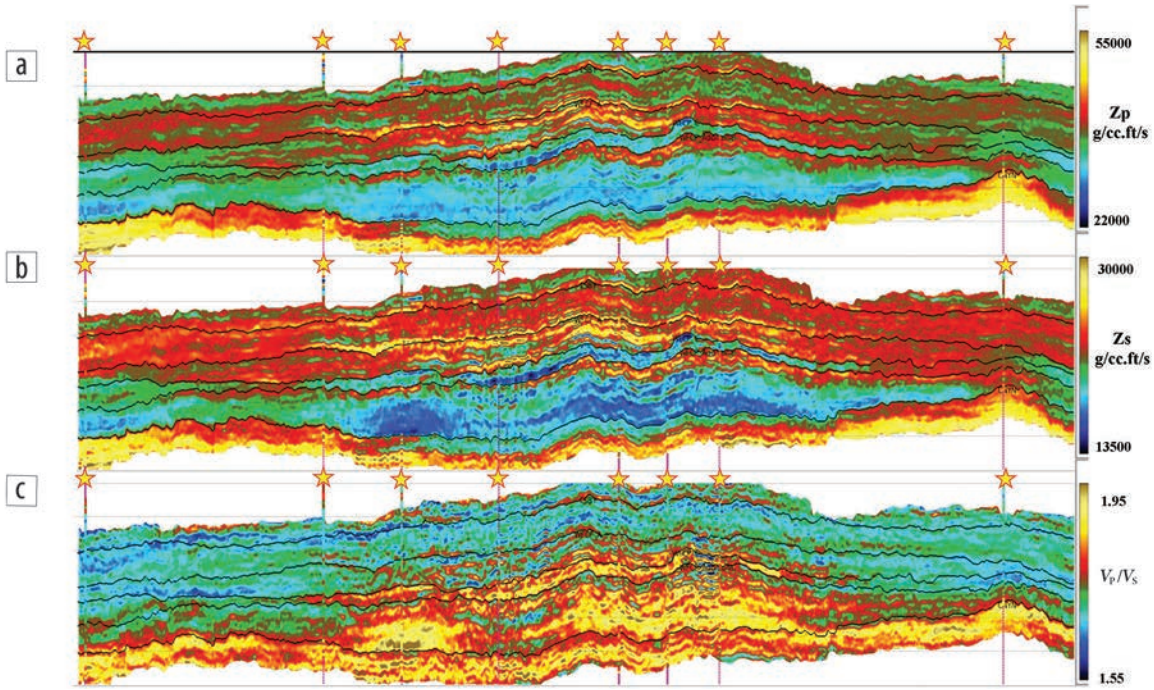

Figure 5. AVO simultaneous inversion output sections. (a) P-impedance, (b) S-impedance, (c) V_P/V_S ratio. Well log measurements are superimposed at locations denoted by stars.

logs. As validation, we computed the correlation coefficient between the inversion output and the measured values at the wells, giving overall correlation coefficients of 94%, 93%, and 89%, respectively, for P-impedance, S-impedance, and V_P/V_S ratio. We then transformed these attributes into lambda rho, mu rho, and Poisson's ratio volumes for use in geomechanical and multiattribute analysis.

Azimuthal inversion. We expanded isotropic seismic inversion by using an anisotropic inversion method to obtain quantitative attributes related to reservoir stress and fractures. Reliable AVAz characterization requires wide-azimuth data acquisition and amplitude-preserved processing, as described in the acquisition and processing section earlier. Unlike previous workflows, this new inversion technique was used to estimate layer-based stress and fracture parameters by deriving effective elastic parameters within an angle azimuth range to mimic the behavior of anisotropic reflection when used in isotropic modeling and inversion.

As in the isotropic case, the azimuthal AVO inversion estimates only fractional band-limited, relative elastic parameters from seismic and requires the anisotropic low-frequency component in order to obtain the full-band, absolute solution. The availability of cross-dipole measurements from boreholes was too sparse to extrapolate an LFM over the survey, so we used the workflow proposed by Mesdag and Quevedo (2017). At first, isotropic inversions were run on each azimuth sector with the isotropic LFM. Then we calculated the azimuthal effective elastic parameters and their corresponding Fourier coefficients over V_P/V_S anisotropy. The low-frequency component is deduced from this first-pass inversion for each of the six azimuthal sectors, and the inversion was then run a second time, with low frequencies in the azimuthal sense, to provide a full-band solution. With the anisotropy magnitude and orientation, assuming the linear slip theory of Schoenberg and Sayers (1995) and the penny-shaped crack model (Hudson, 1980), it is possible to compute the fracture weaknesses, fracture density, and fracture strikes.

Figure 6 shows output of the AVAz inversion: the minimum horizontal stress and the maximum horizontal stress resulting from the combination of AVA and AVAz outputs. Figure 6c shows the distribution of the inverted fracture orientations matching the distributions of orientations measured from formation microimager logs (FMI)

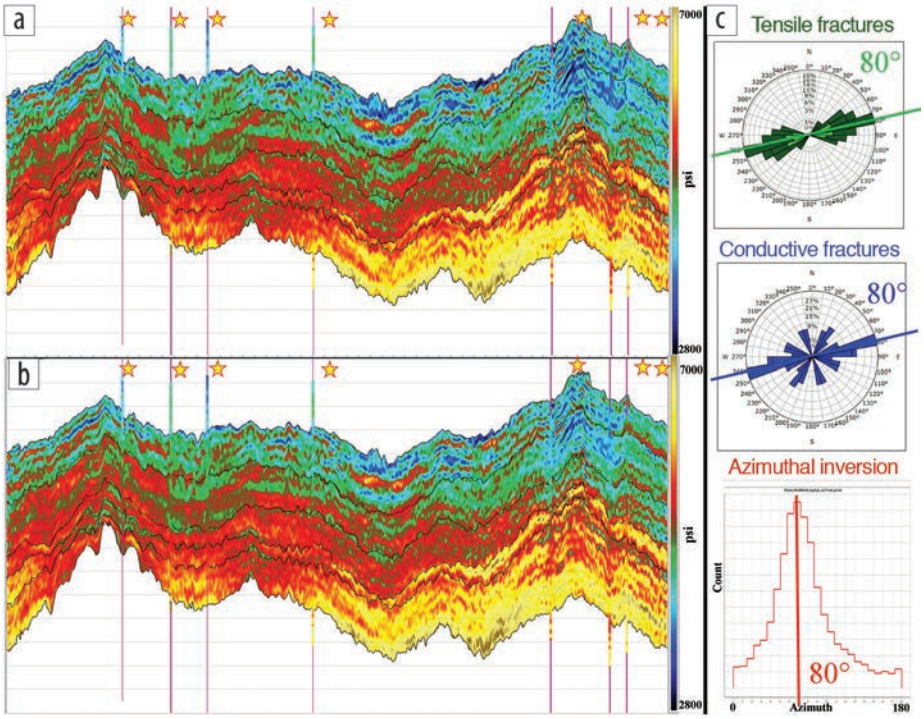

Figure 6. (a) Minimum horizontal stress and (b) maximum horizontal stress obtained through AVAz inversion. (c) Validation: the orientation of fractures obtained by AVAz (bottom in red) match the orientations found at the well on FMI (top in blue and green).

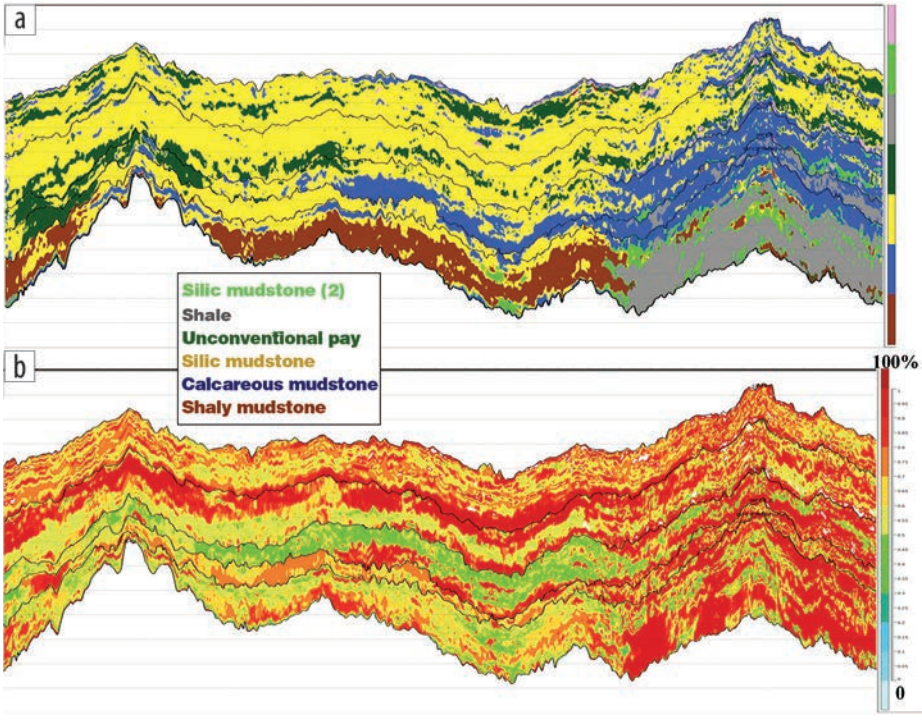

Figure 7. (a) Most probable facies section and (b) the probability of the most probable facies sections.

and serves as a validation of the result. The Spraberry Formation on top shows consistent fracture-induced anisotropy, the Wolfcamp Group below does not exhibit such consistent stress-induced anisotropy. This was confirmed on the two cross-dipole well logs we had available.

Integration

Following the individual rock physics and geophysical inversion sections of the project, we merged the geologic and geophysical products into a data set that has the potential to provide 3D reservoir attributes away from the well control points. A first example consists of a Bayesian facies predictor using the petro-elastic cutoffs defined in the petrophysical analysis. A second application described here is the extrapolation of rock properties away from the wells using multiparameter regression analysis.

Facies prediction. We predicted seismic facies using elastic properties from the simultaneous inversion. The accuracy of the prediction depends on the separation of wireline log facies in the elastic domain at seismic resolution. In this study, six discrete facies were categorized based on different petrophysical cutoffs. Separations of facies were identified by crossplotting various combinations of elastic properties in a 2D domain using different geologic interval-bounded seismic horizons as shown in Figure 3.

P-impedance and V_P/V_S crossplots showed relatively higher separation between facies than other attribute combinations. However, some facies still show overlap in the elastic domain. Therefore, multivariable probability density functions (PDFs) of P-impedance and V_P/V_S for each lithology were computed in each geologic interval. These PDFs and prior probabilities were applied on inverted P-impedance and V_P/V_S volumes using a Bayesian framework. This approach gave posterior probability volumes for each discrete facies. Since it is important for the interpreter to grasp the uncertainty associated with the facies prediction, we output a probability volume for each facies. A section view of the most probable facies volumes is shown in Figure 7, along with its probability at each sample.

Multiattribute analysis. Multiattribute analysis predicts well log properties away from wells in the survey area from inverted properties obtained from seismic. These and their byproducts are referred to as 3D attributes. The analysis data consist of a series of training well logs tied to 3D seismic and elastic attribute volumes. The target logs theoretically may be of any type; however, the greatest success to date has been in predicting porosity logs. The objective is to derive a multiattribute transform, which is a linear or nonlinear transform between a subset of the attributes and the target log values. Once a relationship is found on the well logs, we compute a 3D volume attribute using the seismic inversion volumes.

In this case, an artificial neural network (ANN) was used for the attribute analysis along with standard quality control and calibration between seismic and well data. The selected subset of attributes used for prediction, the features set, is determined by a process of forward stepwise regression, which derives increasingly larger subsets of attributes. Prediction error always decreases as more and more attributes are added to fit the training data. However, this may not be related to an increase in prediction accuracy but may mean that the ANN is overfitting the data as too many attributes are provided for the amount of data. To solve overfitting, we used conventional cross-validation techniques by setting aside some data during the training phase. Once the training is performed, the prediction quality is assessed on this validation data subset. We then displayed the cross-validation error and prediction error as a function of the number of attributes. The cross-validation error decreases at first and starts increasing again; this means we had reached the optimal number of features and overfitting starts to occur, as shown in Figure 8. However, some attributes may not exhibit a reliable predictability. In terms of quality control, it translates into a flat error curve on the training set and a poor correlation at the validation points. This was the case for TOC in this survey. This may be because the training should be distinct for each geologic layer or at the very least distinct for the Wolfcamp and Spraberry, but doing so involved splitting the training data sets in subsets too small for multiattribute regression.

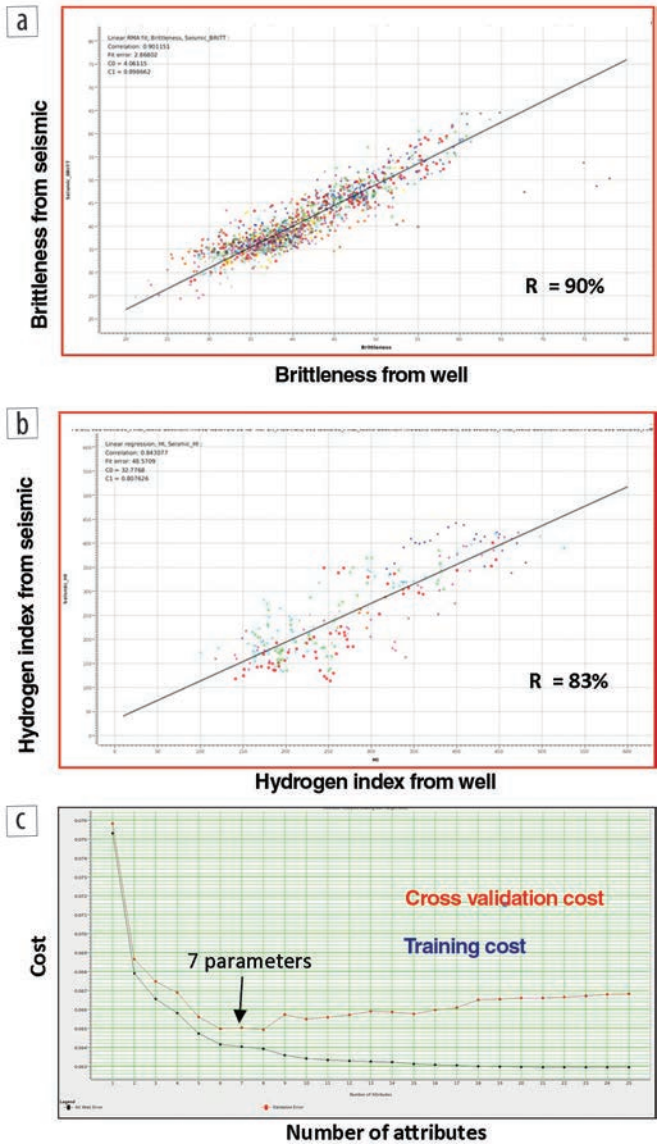

Figure 8. Nonlinear regression quality controls. (a) Brittleness crossplot and (b) hydrogen index and their statistical correlation values. (c) Brittleness cost functions for the training subset and the cross-validation subset of input features.

On a more positive note, we achieved a reliable predictive ability for attributes of several kinds: (1) petrophysical: volume of clay and porosity; (2) geomechanical: brittleness; and (3) geochemical: maturity and hydrogen index, which serves as a proxy for kerogen quality.

Figure 8 shows the crossplots of the validation data for those volumes, the correlation coefficients were 90% and 83%, respectively. Figure 9 shows cross sections of brittleness and kerogen quality volumes obtained.

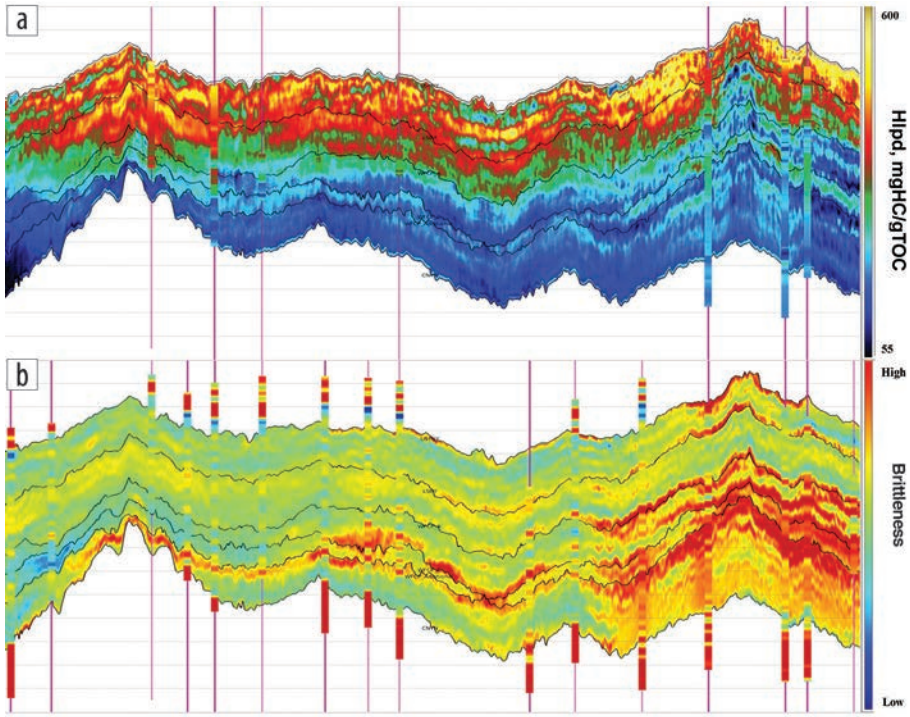

Figure 9. Multiattribute sections through volumes obtained from nonlinear regression. (b) Brittleness and (a) hydrogen index: a proxy for kerogen quality.

Conclusion

For this case study, we implemented a seismic inversion workflow to provide a reservoir model that we then extended with the support of multidisciplinary information that was unique in the area. The adjunction of multidisciplinary geoscience information provided further confidence in our results and allowed for the prediction of rock properties away from the wells on the two formations of interest, the Wolfcamp and the Spraberry.

The addition of different kinds of data has been used in different ways. First, to reduce uncertainty and provide a priori information, the petroelastic model serves to build the LFM. Second, the rock physics data can also be used as validation, for example, when using blind wells during the prestack inversion processes or to check the azimuthal component of LFMs. A third option uses those multidisciplinary attributes as input features for statistical analysis, (1) through empirical relationships for 3D facies prediction in a Bayesian framework or (2) through machine-learning techniques to infer rock properties away from the wells. However, it should be borne in mind that some attributes can lead to poor-quality predictions and that common sense requires enforcing good standards of control through cross validation and abstaining from providing volumes of poor quality when the standards are not met. In this case, we have confidence in our predictions of porosity, volume of clay, brittleness, maturity, and kerogen quality. This means that drilling locations and directions can be chosen with greater certainty. Completion intervals can be chosen for optimum production rather than just placed at regular intervals. Looking forward, we could extend this work further by using Bayesian inversion techniques and geostatistical tools. Similar to the ensemble models computed in meteorology, the geostatistical inversion would compute an ensemble of models based on petrophysics, and whose forward modeling satisfies seismic data. This provides subseismic resolution and a better grasp of uncertainty (Zawila et al., 2015). Another avenue to explore is depth-domain imaging and inversion (Roy et al., 2017). With tighter acquisition parameters, newer processing algorithms, and the possibility of increased well control, we may be able to reap the benefits of having geophysicists and petrophysicists working in the same domain to provide more accurate reservoir mapping. TLE

Acknowledgments

We thank CGG for their permission to publish the paper and CGG Multi-Client and New Ventures for granting us permission to illustrate the paper with examples of their U.S. land data.

Corresponding author: olivier.winter@cgg.com

References

Ashton, T., C. V. Ly, G. Spence, and G. Oliver, 2013, Drilling completion and beyond: RoqSCAN case study from the Barnett/Chester Play: Oilfield Technology, **6**, no. 4.

Berryman, J. G., 1980, Long-wavelength propagation in composite elastic media II: Ellipsoidal inclusions: The Journal of the Acoustical Society of America, **68**, no. 6, 1820–1831, https://doi.org/10.1121/1.385172.

Coulman, T., R. Kenny, S. Rezai, A. Viau, and O. Winter, 2017, Peering into the Permian: Oilfield Technology, **3**, no. 2.

Eaton, B. A., 1976, Using log or seismic data: Graphical method predicts geopressures worldwide: World Oil, 51–56.

Gray, D., P. Anderson, J. Logel, F. Delbecq, D. Schmidt, and R. Schmid, 2012, Estimation of stress and geomechanical properties using 3D seismic data: First Break, **30**, no. 1821, 59–68, https://doi.org/10.3997/1365-2397.2011042.

Hudson, J. A., 1980, Overall properties of a cracked solid: Mathematical Proceedings of the Cambridge Philosophical Society.

Jarvie, D. M., R. J. Hill, T. E. Ruble, and R. M. Pollastro, 2007, Unconventional shale-gas systems: The Mississippian Barnett Shale of North-Central Texas as one model for thermogenic shale-gas assessment: AAPG Bulletin, **91**, no. 4, 475–499, https://doi.org/10.1306/12190606068.

Lacombe, C., G. Gigou, H. Hoeber, A. JafarGandomi, S. De Pierrepont, V. Souvannavong, and J. Verbeke, 2017, Monitoring the quality of prestack broadband seismic data: 87th Annual International Meeting, SEG, Expanded Abstracts, 657–661, https://doi.org/10.1190/segam2017-17722937.1.

Mesdag, P. H., and L. Quevedo, 2017, Quantitative inversion of azimuthal anisotropy parameters from isotropic techniques: The Leading Edge, **36**, no. 11, 916–923, https://doi.org/10.1190/tle36110916.1.

Mitchell, W. K., and R. J. Nelson, 1988, A practical approach to statistical log analysis: Presented at SPWLA 29th Annual Logging Symposium.

Peake, N., G. Castillo, N. Van de Coevering, S. Voisey, A. Bouziat, K. Chesser, G. Oliver, C. Vinh Ly, and R. Mayer, 2014, Integrating surface seismic, microseismic, rock properties and mineralogy in the Haynesville Shale: Unconventional Resources Technology Conference, 343–353.

Poupon, A., and J. Leveaux, 1971, Evaluation of water saturation in shaly formations: Presented at SPWLA 12th Annual Logging Symposium.

Roy, A., L. Zheng, X. Hu, R. Pearson, E. Oropeza, S. Mueller, and M. Chang, 2017, Anisotropic prestack depth-migration processing in the Permian Basin, Texas: 87th Annual International Meeting, SEG, Expanded Abstracts, 3997–4001, https://doi.org/10.1190/segam2017-17791539.1.

Russell, B., and D. Hampson, 1991, A comparison of post-stack seismic inversion methods: 61st Annual International Meeting, SEG, Expanded Abstracts, 876–878.

Sayers, C., and S. Dean, 2001, Azimuth-dependent AVO in reservoirs containing non-orthogonal fracture sets: Geophysical Prospecting, **49**, no. 1, 100–106, https://doi.org/10.1046/j.1365-2478.2001.00236.x.

Schmoker, J. W., 1979, Determination of organic content of Appalachian Devonian shales from formation density logs: AAPG Bulletin, **63**, no. 9, 1504–1509.

Schoenberg, M., and C. M. Sayers, 1995, Seismic anisotropy of fractured rock: Geophysics, **60**, no. 1, 204–211, https://doi.org/10.1190/1.1443748.

Simandoux, P., 1963, Dielectric measurements on porous media application to the measurement of water saturations: Study of the behavior of argillaceous formations: Revue de l'Institut Francais du Petrole, **18**, 193–215.

Wang, S., and D. Wilkinson, 2012, Imaging for unconventional resource plays using an orthorhombic velocity model: 82nd Annual International Meeting, SEG, Expanded Abstracts, 1–5, https://doi.org/10.1190/segam2012-0788.1.

Yates, M., G. Byerley, R. Eden, D. Monk, and S. Voisey, 2016, An Oklahoma broadband land seismic case history: 86th Annual International Meeting, SEG, Expanded Abstracts, 5104–5108, https://doi.org/10.1190/segam2016-13871103.1.

Zawila, J., S. Fluckiger, G. Hughes, P. Kerr, A. Hennes, M. Hofmann, H. Wang, and H. Titchmarsh, 2015, An integrated, multidisciplinary approach utilizing stratigraphy, petrophysics, and geophysics to predict reservoir properties of tight unconventional sandstones in the Powder River Basin, Wyoming, USA: 85th Annual International Meeting, SEG, Expanded Abstracts, 2677–2681, https://doi.org/10.1190/segam2015-5852423.1.